

Significant Elevation in Potassium Concentration Surrounding Stimulated Excitable Cells Revealed by an Aptamer-Modified Nanowire Transistor

Ankur Anand, Hui-Chiun Tseng, Hsu-Cheng Chiang, Wan-Hsuan Hsu, Yi-Fan Liao, Serena Huei-An Lu, Su-Yi Tsai, Chien-Yuan Pan,* and Yit-Tsong Chen*



Cite This: *ACS Appl. Bio Mater.* 2021, 4, 6865–6873



Read Online

ACCESS |



Metrics & More

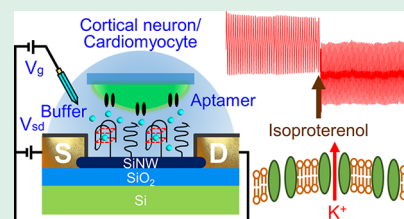


Article Recommendations



Supporting Information

ABSTRACT: Recording ion fluctuations surrounding biological cells with a nano-electronic device offers seamless integration of nanotechnology into living organisms and is essential for understanding cellular activities. The concentration of potassium ion in the extracellular fluid ($C_{K^+}^{ex}$) is a critical determinant of cell membrane potential and must be maintained within an appropriate range. Alteration in $C_{K^+}^{ex}$ can affect neuronal excitability, induce heart arrhythmias, and even trigger seizure-like reactions in the brain. Therefore, monitoring local fluctuations in real time provides an early diagnosis of the occurrence of the K^+ -induced pathophysiological responses. Here, we modified the surface of a silicon nanowire field-effect transistor (SiNW-FET) with K^+ -specific DNA-aptamers (Apt_{K^+}) to monitor the real-time variations of $C_{K^+}^{ex}$ in primary cultured rat embryonic cortical neurons or human embryonic stem cell-derived cardiomyocytes. The binding affinity of Apt_{K^+} to K^+ , determined by measuring the dissociation constant of the $Apt_{K^+}-K^+$ complex ($K_d = 10.1 \pm 0.9$ mM), is at least 38-fold higher than other ions (e.g., Na^+ , Ca^{2+} , and Mg^{2+}). By placing cultured cortical neurons over an $Apt_{K^+}/SiNW-FET$ device, α -amino-3-hydroxy-5-methyl-4-isoxazolepropionic acid (AMPA) stimulation raised the $C_{K^+}^{ex}$ dose-dependently to 16 mM when AMPA concentration was $>10 \mu M$; this elevation could be significantly suppressed by an AMPA receptor antagonist, 6,7-dinitroquinoxaline-2,3-dione. Likewise, the stimulation of isoproterenol to cardiomyocytes raised the $C_{K^+}^{ex}$ to 6–8 mM, with a concomitant increase in the beating rate. This study utilizing a robust nanobiosensor to detect real-time ion fluctuations surrounding excitable cells underlies the importance of ion homeostasis and offers the feasibility of developing an implant device for real-time monitoring.



KEYWORDS: aptamer, cardiomyocyte, excitability, extracellular K^+ concentration, membrane potential, nanowire field-effect transistor

INTRODUCTION

Ion homeostasis is a fundamental biological property and is involved in a variety of physiological functions. The extracellular K^+ concentration ($C_{K^+}^{ex}$) is essential in regulating resting membrane potential and cell excitability.¹ At the recovery phase of an action potential, K^+ flows out of the cells to repolarize the membrane potential.² Due to the limited space among neurons in the nervous tissue, this K^+ efflux will elevate the $C_{K^+}^{ex}$ and shift the equilibrium potential of K^+ positively. The change in $C_{K^+}^{ex}$ (denoted by $\Delta C_{K^+}^{ex}$) by a millimolar (mM) level in several regions of the brain regulates neuronal excitability and the sleep–wake cycle.³ In the nervous system, glial cells play an important role in buffering the $C_{K^+}^{ex}$ to modulate neural network oscillations and synchrony.⁴ Abnormality in buffering the $C_{K^+}^{ex}$ and maintaining the ion homeostasis may cause neuropathies, like epilepsy and Alzheimer's disease.⁵

Some studies adopting a microdialysis probe technique have shown that $C_{K^+}^{ex}$ can increase by several mM in the interstitial milieu of muscle and brain.^{6,7} However, this technique lacks the spatial and temporal resolutions that are required for real-

time probing the local changes of $C_{K^+}^{ex}$ at the membrane surface. For neurons, the supports for the importance of $C_{K^+}^{ex}$ homeostasis in modulating neuronal network activities come mostly from computational models. Depending on the parameters adopted in the model calculations, the $\Delta C_{K^+}^{ex}$ reported to affect the action potential firing pattern varies from the sub mM to 10 mM level.^{8,9} Apparently, knowing the exact value of $C_{K^+}^{ex}$ at rest or during excitation is crucial in characterizing the activities of excitable cells under normal or abnormal conditions.

Here, we linked the surface of a multiple-parallel-connected (MPC) silicon nanowire field-effect transistor (SiNW-FET) with aptamers, which can bind K^+ specifically, (denoted by Apt_{K^+} with the DNA sequence of 3'-

Received: May 20, 2021

Accepted: August 15, 2021

Published: August 27, 2021



GGTTGGTGTGGTTGGATTTT-5') to monitor the elevation of $C_{K^+}^{ex}$ due to the release of K^+ from living cells. The SiNW-FET is an extremely sensitive device for sensing the receptor–target interactions,^{10–14} electrical responses of neurons,¹⁵ and minute signaling molecules released from excitable cells.¹⁶ The Apt_{K⁺} selected here is a single-strand DNA with binding affinity to K^+ at a mM range, allowing the Apt_{K⁺}-modified SiNW-FET (referred to as Apt_{K⁺}/SiNW-FET) for the detection of $\Delta C_{K^+}^{ex}$ at physiological conditions.¹⁷ Our results showed that the $\Delta C_{K^+}^{ex}$ of cultured embryonic cortical neurons could reach 8–16 mM when stimulated by α -amino-3-hydroxy-5-methyl-4-isoxazolepropionic acid (AMPA) with a concentration (C_{AMPA}) of $>10 \mu M$. In addition, by placing the cultured cardiomyocytes (derived from human embryonic stem cells (hESC)) with spontaneous beating activity onto an Apt_{K⁺}/SiNW-FET device, we observed an escalated $C_{K^+}^{ex}$ with an increasing concomitant beating frequency. The $C_{K^+}^{ex}$ of the cultured excitable cells under repetitive or potent stimulation can ascend to a high enough level to affect the membrane potential to regulate cell excitability. Consequently, our device cannot only monitor the real-time biomolecular changes, but also offer the feasibility of developing an implantable device for early diagnosis.

RESULTS AND DISCUSSION

Sensitivity and Specificity of an Apt_{K⁺}/SiNW-FET. To detect the $C_{K^+}^{ex}$ surrounding cultured cortical neurons or cardiomyocytes, a coverslip containing cultured cells was laid on top of an Apt_{K⁺}/SiNW-FET device to allow the cells to have close contact with the device surface, as depicted in Figure 1. A single chip includes six MPC SiNW-FET devices, each of which contains as many as tens of p-type single-crystalline boron-doped SiNWs laid underneath an array of interdigitated source-drain electrodes (Figure 1b and the electrical characterizations in Figure S1 of the Supporting Information). The SiNW-FETs exhibited an ohmic contact as demonstrated in a measured output curve [i.e., the source-drain current vs bias voltage ($I_{sd}-V_{sd}$) plot in Figure S1c] and a high transconductance of $\sim 2.1 \mu S$ as derived from a measured transfer curve [i.e., the source-drain current vs gate voltage ($I_{sd}-V_g$) plot in Figure S1d].

The concentrations of K^+ and Na^+ in the extracellular milieu are typically ~ 5 and ~ 140 mM, respectively. To effectively probe the $\Delta C_{K^+}^{ex}$, the Apt_{K⁺} selected in this study has been reported to form a G-quadruplex structure driven preferentially by K^+ ions with the dissociation constant of $K_d \sim 14$ mM.^{17,18} To characterize the sensitivity of an Apt_{K⁺}/SiNW-FET against K^+ , we perfused the Apt_{K⁺}/SiNW-FET device with Tris buffer (10 mM, pH 7.4) containing different concentrations of K^+ (denoted by C_{K^+}) via polydimethylsiloxane (PDMS) microfluidic channel coupled to the device. The measured transfer curves of an Apt_{K⁺}/SiNW-FET relative to different $C_{K^+} = 1 \mu M$ to 300 mM are plotted in Figure 2a. As C_{K^+} rises, the transfer curves move further down, revealing the electrostatic gating effect on the p-type SiNW-FET device. To avoid device-to-device variations, we converted the changes in I_{sd} (i.e., ΔI_{sd}) at a specified V_g with respect to the buffer solution, into corresponding changes in V_g (referred to as a calibrated response, $\Delta V_{g,K^+}^{cal}$) based on the transfer curve of the FET device utilized (as displayed in Figure S3).^{16,19} We then normalized the $\Delta V_{g,K^+}^{cal}$, calculated from the values measured in

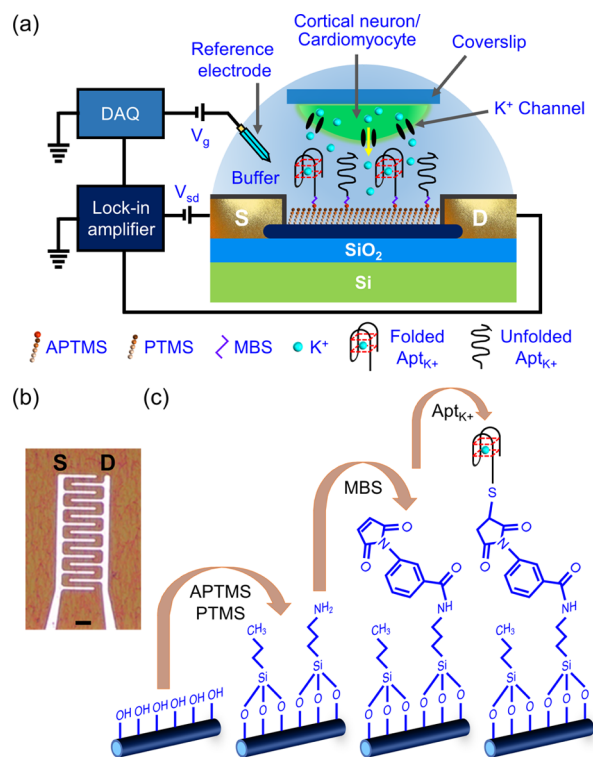


Figure 1. Experimental setup of an Apt_{K⁺}/SiNW-FET sensor for the detection of K^+ ions. (a) Schematic depiction of the use of an Apt_{K⁺}/SiNW-FET to monitor the K^+ ions effluxed from cultured cortical neurons/cardiomyocytes. A MPC SiNW-FET device was modified with Apt_{K⁺} (referred to as Apt_{K⁺}/SiNW-FET) and encompassed by a PDMS wall/microfluidic channel filled with buffer solution. A neuron-seeded coverslip was placed on top of the Apt_{K⁺}/SiNW-FET device allowing neurons in intimate contact with the Apt_{K⁺}/SiNW-FET surface. A Ag/AgCl reference electrode was used as a solution gate for supplying gate voltage in the transfer-curve scans and was held at ground potential throughout biosensing measurements. Upon stimulation, the K^+ ions released from cortical neurons were captured by Apt_{K⁺}/SiNW-FET to cause conductance change in the MPC SiNW-FET, of which the signal was collected by a lock-in amplifier. (b) Optical image of a MPC SiNW-FET device. Tens to hundreds of SiNWs were entrapped beneath and placed amid the interdigitated source (S) and drain (D) electrodes. Scale bar: 10 μm . (c) A chemical procedure of immobilizing Apt_{K⁺} (3'-GGTTGGTGTGGTTGGATTTT-SH-5') on a MPC SiNW-FET device (with the details described in the Experimental Section). First, the SiNW surface was modified with APTMS and PTMS in a molar ratio of 1:5. Next, MBS was applied as a cross-linker to immobilize Apt_{K⁺} with the APTMS. The drawing is not to scale.

Figure 2a at $V_g = 0$ mV, to the maximum (saturated) response at $C_{K^+} \geq 100$ mM (referred as $\Delta V_{g,K^+}^{cal}/\Delta V_{g,K^+}^{cal,max}$) and plotted $\Delta V_{g,K^+}^{cal}/\Delta V_{g,K^+}^{cal,max}$ against C_{K^+} (Figure 2b). The curve in Figure 2b shows a rapid escalation in $\Delta V_{g,K^+}^{cal}/\Delta V_{g,K^+}^{cal,max}$ as C_{K^+} increases from 0 to 50 mM and then reaches a plateau afterward. We plotted the $C_{K^+}/\Delta V_{g,K^+}^{cal}$ versus C_{K^+} graph (in the inset of Figure 2b) and fitted the curve with a least-squares Langmuir adsorption isotherm model (Section S2, Supporting Information),¹⁶ rendering $K_d = 10.1 \pm 0.9$ mM for the K^+ -Apt_{K⁺} complex, which is similar to the previously reported value of 14 mM.¹⁷ For a control test, a MPC SiNW-FET device modified only with propyltrimethoxysilane (PTMS) but

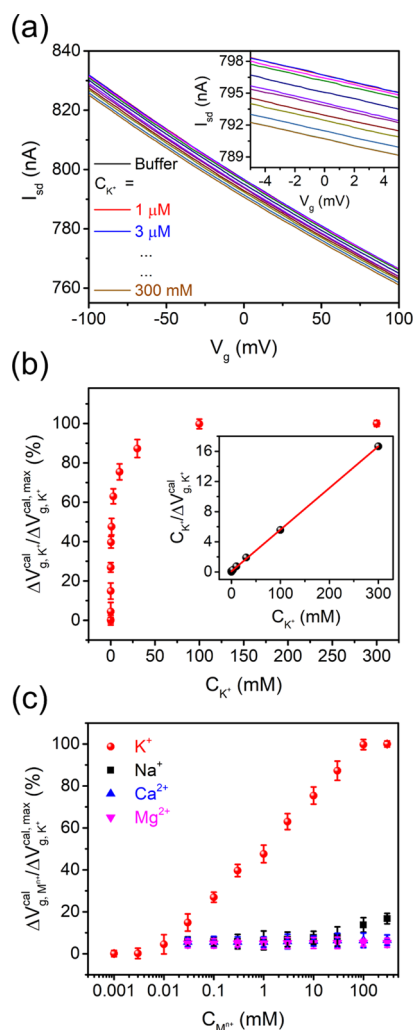


Figure 2. Apt_{K⁺}/SiNW-FET was demonstrated to capture K⁺ ions with high target selectivity and hold superior binding affinity against other metal ions. (a) Transfer curves (I_{sd} – V_g) of an Apt_{K⁺}/SiNW-FET were scanned in response to various C_{K^+} . (b) Plot of the normalized calibrated response of $\Delta V_{g,K^+}^{cal}/\Delta V_{g,K^+}^{cal,max}$ as a function of C_{K^+} . The $\Delta V_{g,K^+}^{cal,max}$ reflects the maximum (saturated) electrical response of the Apt_{K⁺}/SiNW-FET attained when $C_{K^+} \geq 100$ mM. The inset shows the fitting result of the data with the Langmuir adsorption isotherm model to yield $K_d = 10.1 \pm 0.9$ mM for the K⁺–Apt_{K⁺} complex. (c) Apt_{K⁺}/SiNW-FET device was employed to detect different metal ions ($M^{n+} = K^+, Na^+, Ca^{2+},$ or Mg^{2+}) at various concentrations. The test shows the excellent selectivity of an Apt_{K⁺}/SiNW-FET for detecting K⁺. The data points of panels (b) and (c) represent the mean \pm SD of three independent experiments.

without Apt_{K⁺} (denoted by PTMS/SiNW-FET) was employed for detecting K⁺; the resultant transfer curves revealed no evident reaction to K⁺ at $C_{K^+} = 1 \mu$ M to 300 mM (Figure S4). The outcome of these measurements suggests that the changes in conductance detected by Apt_{K⁺}/SiNW-FET are due to the binding of K⁺ onto the Apt_{K⁺} modified on the SiNW-FET surface.

In addition to K⁺, a biological buffer usually contains various ions of different concentrations. To verify the target specificity of this Apt_{K⁺}/SiNW-FET device, we perfused an Apt_{K⁺}/SiNW-FET device with 10 mM of Tris buffer containing various ions (K⁺, Na⁺, Ca²⁺, or Mg²⁺) and measured the change in

conductance (Figure 2c). When the normalized $\Delta V_{g,M^{n+}}^{cal}/\Delta V_{g,K^+}^{cal,max}$ is plotted against different ions ($C_{M^{n+}}$ with $M^{n+} = K^+, Na^+, Ca^{2+},$ or Mg^{2+}), the results showed that Mg²⁺ and Ca²⁺ do not cause an appreciable conductance change; in contrast, Na⁺ has a slight affinity to the Apt_{K⁺} ($K_d = 387.8 \pm 21.7$ mM), but \sim 38-fold lower than K⁺. Most G-quadruplexes are known to exhibit a modest binding affinity to Na⁺, although it is substantially weaker than K⁺.²⁰ Overall, the Apt_{K⁺}/SiNW-FET sensor has a linear working range of detecting K⁺ from 0.03 to 30 mM (Figure 2c). Consequently, this Apt_{K⁺}/SiNW-FET with the target-specific capability is well suited for detecting the variations of C_{K^+} in a physiological medium composed of distinct biological ions.

To determine the interference of Na⁺ on the binding of K⁺ onto the Apt_{K⁺}/SiNW-FET, we prepared buffers containing a mixture of K⁺ and Na⁺ in varied concentration ratios (while the overall ionic strength is constant), that is, K⁺/Na⁺ = 0:10, 1:9, 3:7, 5:5, 7:3, 9:1, and 10:0 (in mM units), respectively. Figure S5a demonstrates that the higher the K⁺/Na⁺ ratio in the mixed K⁺/Na⁺ solution, the more downward shift of the transfer curve, and the conductance change of the Apt_{K⁺}/SiNW-FET exhibits a linear response with the increasing fraction of K⁺ (Figure S5b). This linear response implies that the C_{K^+} is predominantly responsible for the conductance change of an Apt_{K⁺}/SiNW-FET. With a quantitative calibration before cell experiments, this Apt_{K⁺}/SiNW-FET sensor is legitimate to measure C_{K^+} in a biological mixture even in the presence of excessive Na⁺.

AMPA Stimulation Elevates the $C_{K^+}^{ex}$ Surrounding Cultured Neurons. In the brain, the astrocytes regulate the local $C_{K^+}^{ex}$ via the K⁺ spatial buffering mechanism to modulate neuronal excitability.⁴ The change in $C_{K^+}^{ex}$ will shift the equilibrium potential of K⁺ positively or negatively, resulting in adjusting the resting membrane potential.²¹ To verify that the K⁺ efflux can cause a significant local $\Delta C_{K^+}^{ex}$ to affect the resting membrane potential, we put a coverslip with the side seeded with cultured neurons facing an Apt_{K⁺}/SiNW-FET circuit and added AMPA into the reservoir containing Hank's balanced salt solution (HBSS) (Figure 1a). There are at least three subtypes of ion channel-conjugated glutamate receptors according to the binding of a specific agonist. AMPA is an agonist of the AMPA receptor (AMPA), which is involved in the excitatory neurotransmission of the central nervous system.²² The activation of AMPAR, as shown in Figure 3a, enables the Na⁺ fluxing into the cytosol and depolarizes the membrane potential. This depolarization will in turn activate the voltage-gated Na⁺ channels (VGSC) and further bring the membrane potential transiently approaching the equilibrium potential of Na⁺, which is usually at \sim 50 mV under physiological conditions. Such strong depolarization will then activate the voltage-gated K⁺ channels (VGPC) and cause the K⁺ fluxing out of a cell, giving rise to the elevation of $C_{K^+}^{ex}$ and subsequent membrane repolarization. In the meantime, K⁺ will also flux through the AMPARs.

In this study, we added AMPA of different concentrations ($C_{AMPA} = 0.1, 0.3, 1, 3, 5, 7, 10, 13, 15, 17,$ and 20μ M) to stimulate cortical neurons and monitored the conductance changes of the Apt_{K⁺}/SiNW-FET sensor to determine the released $C_{K^+}^{ex}$. To correlate the electrical response of Apt_{K⁺}/SiNW-FET to C_{K^+} , we immersed the device in HBSS (which contained 5.8 mM K⁺ originally) and increased the C_{K^+}

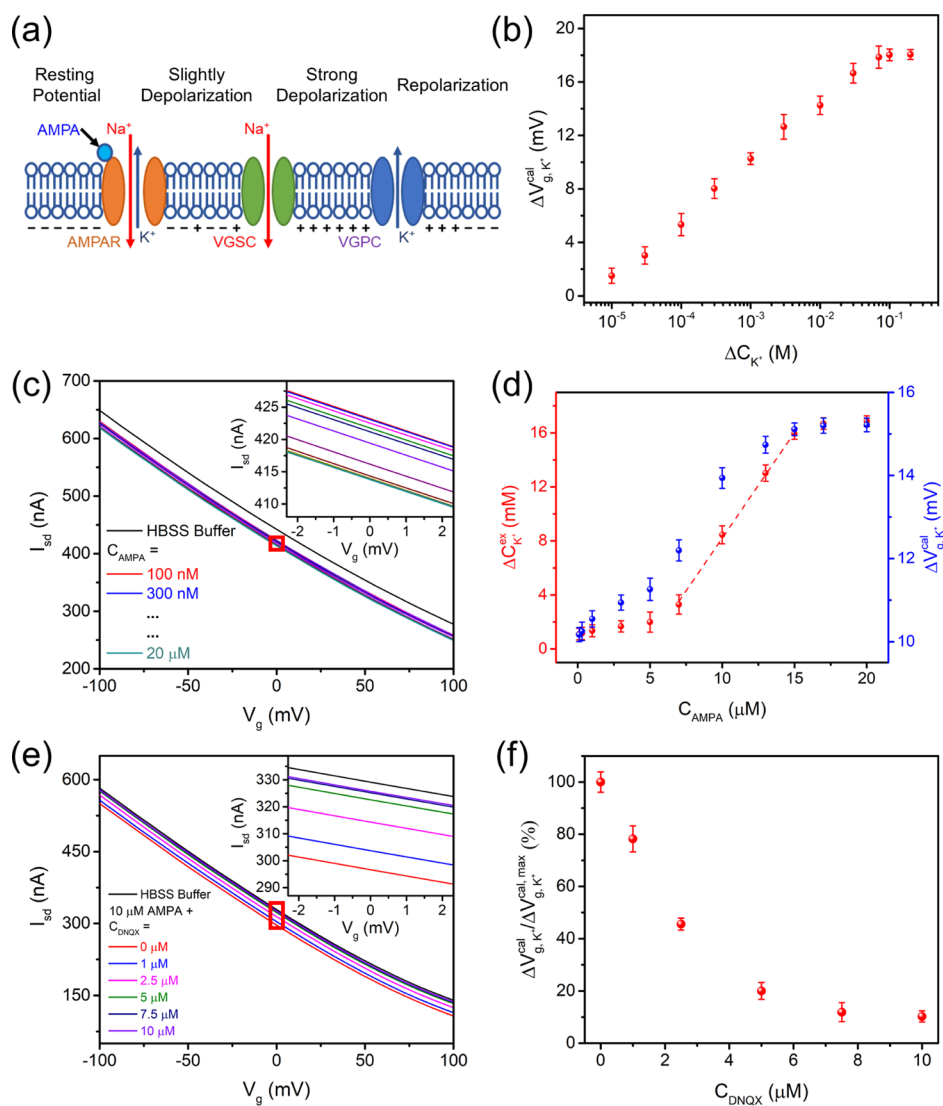


Figure 3. Apt_K⁺/SiNW-FET was used to detect the K⁺ release from stimulated neurons. The neurons cultured on a glass coverslip were laid on top of an Apt_K⁺/SiNW-FET and were treated with various C_{AMPA}, while the K⁺ efflux was monitored by Apt_K⁺/SiNW-FET. (a) AMPA stimulation will lead to the membrane depolarization and activate voltage-gated Na⁺ and K⁺ channels (denoted by VGSC and VGPC, respectively). K⁺ will then efflux *via* the K⁺ channels and AMPARs to elevate C_K^{ex}. (b) Calibration plot. Prior to cell experiments, the electrical response of an Apt_K⁺/SiNW-FET to different C_K⁺ (10 μM to 300 mM) in HBSS was measured. This calibration plot was obtained by measuring the transfer curves at different C_K⁺ and transforming the data to the ΔV_{g,K}^{cal} vs ΔC_K⁺ plot as the procedures implemented in Figure 2a,b. It should be noted that the original HBSS buffer contained 5.8 mM K⁺, to which various C_K⁺ (10 μM to 300 mM) was added to construct the calibration curve. (c) Shift of a transfer curve by AMPA stimulation. The transfer curves of a neuron-covered Apt_K⁺/SiNW-FET were scanned with the neurons stimulated with different doses of C_{AMPA} at 100 nM to 20 μM in HBSS. The inset shows the magnification of the transfer curves marked within a red square between V_g = −2 and 2 V. (d) ΔC_K^{ex} was measured in the vicinity of neurons. The ΔV_{g,K}^{cal} [right ordinate, blue circles, with the data taken from panel (c)] was transformed to ΔC_K^{ex} (left ordinate, red circles) based on the calibration curve presented in panel (b). The red dashed line is drawn as a guide to the eye. (e) DNQX suppresses the AMPA-evoked response. The transfer curves of a neuron-covered Apt_K⁺/SiNW-FET were scanned with the neurons pretreated with DNQX (1–10 μM) for 10 min prior to the application of AMPA (10 μM). The inset is the magnification of the transfer curves marked within a red square between V_g = −2 and 2 V. (f) Inhibitory effect of DNQX is dose-dependent. The normalized calibrated responses (ΔV_{g,K}^{cal}/ΔV_{g,K}^{cal,max}) of the neuron-covered Apt_K⁺/SiNW-FET were plotted against C_{DNQX} in which the ΔV_{g,K}^{cal}/ΔV_{g,K}^{cal,max} values were converted from the transfer curves measured in panel (e). The data shown in panels b,d,f represent the mean ± SD from at least three measurements.

gradually prior to the cell experiment (Figure 3b). The initial value of the calculated ΔV_{g,K}^{cal} indicates the background response of the device to the 5.8 mM of K⁺ in the HBSS. While plotting the calculated ΔV_{g,K}^{cal} against the added C_K⁺ (i.e., ΔC_K⁺, on top of the 5.8 mM in HBSS), the curve shows a linear relationship from 10^{−5} to 7 × 10^{−2} M and becomes saturated

after 10^{−1} M. In the absence of neurons, AMPA did not elicit any response from the Apt_K⁺/SiNW-FET (Figure S6a). When placing neurons on top of the Apt_K⁺/SiNW-FET, the electrical responses (I_{sd}) decreased as C_{AMPA} increased (Figure 3c). With the aid of the calibration curve (Figure 3b), the calculated ΔV_{g,K}^{cal} from the curves of Figure 3c (presented in the right ordinate of Figure 3d) under different C_{AMPA} was converted to

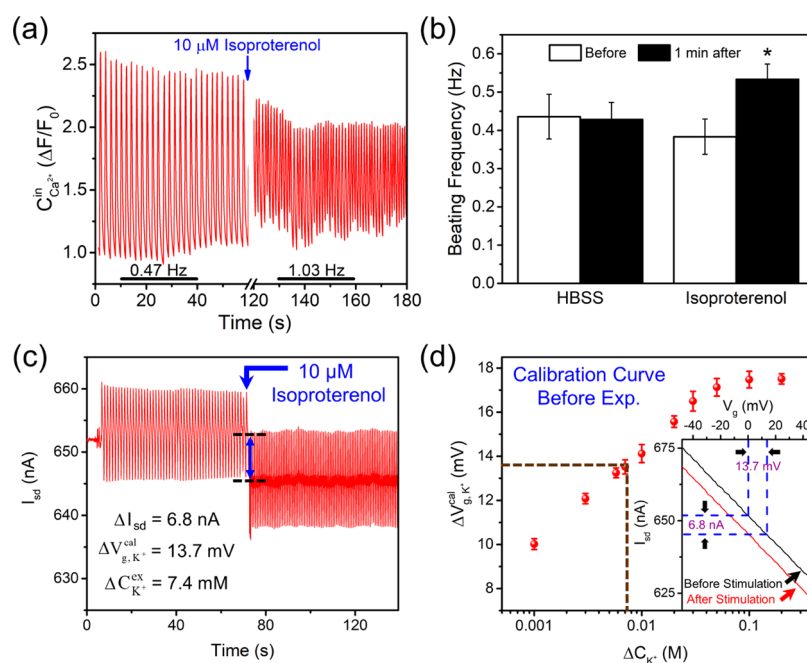


Figure 4. Isoproterenol stimulation increases the beating frequency and $C_{K^+}^{ex}$ of the cultured cardiomyocytes differentiated from hESC. (a,b) Cultured cardiomyocytes were loaded with Fluo-2, and the changes in the fluorescence intensity were measured to represent the changes in $C_{Ca^{2+}}^{in}$. (a) Representative real-time response of $C_{Ca^{2+}}^{in}$ from the cultured cardiomyocytes. Isoproterenol ($10 \mu M$) was added at the 60th s. The beating frequencies before and after the isoproterenol treatment were calculated from a 30 s period at 10–40 and 130–160 s, respectively. (b) Average beating frequencies before and after the HBSS ($n = 8$) and isoproterenol treatment ($n = 7$). The data presented are mean \pm SD, and * represents $p < 0.05$ with the Student's t -test. (c,d) Cardiomyocytes cultured on a coverslip were placed on top of an $Apt_{K^+}/SiNW$ -FET and stimulated with isoproterenol ($10 \mu M$) in HBSS. (c) I_{sd} vs elapsed time curve of the $Apt_{K^+}/SiNW$ -FET device in close contact with cardiomyocytes indicates that the isoproterenol application (indicated by an arrow) decreased the average ΔI_{sd} by 6.8 nA (marked by a blue double arrow). (d) Before cell experiments, the electrical response of the $Apt_{K^+}/SiNW$ -FET was calibrated against various ΔC_{K^+} (1–200 mM) in HBSS. In the inset, $\Delta I_{sd} = 6.8$ nA after the isoproterenol stimulation [measured in Panel (c)] is converted to $\Delta V_{g,K^+}^{cal} = 13.7$ mV. This $\Delta V_{g,K^+}^{cal} = 13.7$ mV corresponds to $\Delta C_{K^+}^{ex} = 7.4$ mM (guided by the brown dashed lines) released from the stimulated cardiomyocytes.

the change in $C_{K^+}^{ex}$ (i.e., $\Delta C_{K^+}^{ex}$, in the left ordinate of Figure 3d). As seen in Figure 3d, apart from the original $C_{K^+} = 5.8$ mM that existed in the HBSS buffer, the $\Delta C_{K^+}^{ex}$ increased only by 1–2 mM after the cortical neurons were stimulated with $C_{AMPA} \leq 5 \mu M$. With stronger stimulations of $C_{AMPA} = 7$ – $15 \mu M$, the $\Delta C_{K^+}^{ex}$ increased quite linearly and reached a saturation level of ~ 16 mM at $C_{AMPA} > 15 \mu M$. The half-maximal effective concentration (EC_{50}) of AMPA for increasing $C_{K^+}^{ex}$ is $8.9 \pm 0.9 \mu M$ (Section S3 of the Supporting Information), which is consistent with the previously cited EC_{50} of 11– $17 \mu M$ by measuring the electric currents in neurons isolated from the spinal cord or brain.²²

To verify that the AMPA-triggered conductance changes were affected by the AMPAR, the neurons were pretreated with 6,7-dinitroquinoxaline-2,3-dione (DNQX) before AMPA stimulation (Figure 3e,f). DNQX is an antagonist of AMPAR with a half-maximal inhibitory concentration (IC_{50}) of $\sim 0.5 \mu M$.²³ While DNQX did not evoke any significant response from an $Apt_{K^+}/SiNW$ -FET without neurons (Figure S6b), the AMPA-induced $C_{K^+}^{ex}$ from the DNQX-pretreated neurons diminished, as revealed by the decreased downshifts of the transfer curves (Figure 3e). In Figure 3f, the normalized electrical responses (with the experimental data taken from Figure 3e) reveal that the DNQX pretreatment significantly suppressed the AMPA-induced conductance changes (i.e., the $C_{K^+}^{ex}$ releases) in a dose-dependent manner, where the suppression reached a maximal inhibitory effect at $C_{DNQX} >$

$7 \mu M$. These results support that the AMPA-evoked conductance change is facilitated through the activation of AMPAR.

Our previous report has shown that an AMPA stimulation to the neurons in a Na^+ -devoid buffer can only elevate $C_{K^+}^{ex}$ by $\sim 1 \mu M$.¹⁵ In such a condition, there is no strong depolarization induced by the influx of Na^+ via both AMPAR and VGSC to activate VGPC; therefore, only a few K^+ ions efflux from neurons via AMPAR. In this study, neurons were bathed in a normal physiological buffer that contained ~ 143 mM Na^+ ; when these neurons were treated with AMPA, the Na^+ influx via AMPAR sufficiently depolarized the membrane potential, resulting in the activations of both VGSC and VGPC. Subsequently, abundant K^+ exits the cell resulting in the escalation of $\Delta C_{K^+}^{ex}$ to ~ 16 mM (as shown in Figure 3d). These results suggest that our $Apt_{K^+}/SiNW$ -FET device is a viable sensor for evaluating the activities of those ion channels in excitable cells.

Significant K^+ Efflux from Embryonic Stem Cell-Derived Cardiomyocytes. To further demonstrate the capability of $Apt_{K^+}/SiNW$ -FETs in investigating cellular activities, we differentiated hESC to cardiomyocytes on a coverslip, which was then placed on top of an $Apt_{K^+}/SiNW$ -FET device with the cells facing the device circuit. The cultured cardiomyocytes showed repetitive spontaneous contraction as displayed in their morphological changes and the frequency varies batch by batch (Supplementary Video 1).

Such contraction involves a series of steps similar to the action potential firing and requires an elevation in the intracellular Ca^{2+} concentration ($C_{\text{Ca}^{2+}}^{\text{in}}$) to trigger the contraction.²⁴ By loading the cells with Fluo2, a Ca^{2+} -sensitive fluorescence dye, we recorded the changes in fluorescence intensities to represent the responses of $C_{\text{Ca}^{2+}}^{\text{in}}$ before (Supplementary Video 2) and after (Supplementary Video 3) the application of isoproterenol (10 μM).^{25,26} Isoproterenol is a non-selective β adrenoreceptor agonist that can enhance the beating frequency of hESC-derived cardiomyocytes with an EC_{50} of 12.9 nM.²⁷ In Figure 4a, the normalized fluorescence intensities from a group of cells exhibit the rise and fall of repetitive signals with a frequency of 0.47 Hz at the beginning of the recording; comparatively, the repetition rate increased to 1.03 Hz at 1 min after the application of 10 μM isoproterenol. In Figure 4b, differentiated cardiomyocytes were stimulated with HBSS and isoproterenol, respectively; while HBSS application had no effect on the beating frequency (0.44 ± 0.06 vs 0.43 ± 0.04 Hz, $n = 8$), isoproterenol significantly increased the frequency from 0.38 ± 0.05 Hz right before the stimulation to 0.53 ± 0.04 Hz at 1 min after the drug application ($n = 7$, $p < 0.05$).

Similar to neurons, the K^+ efflux *via* VGPC repolarizes the membrane potential during the recovery phase of heart contraction in cardiac cells.^{28,29} In Figure 4c, the electrical response of a cardiomyocyte-covered $\text{Apt}_{\text{K}^+}/\text{SiNW-FET}$ appeared in the form of transient spikes with a frequency of 0.79 Hz; after the application of isoproterenol, the frequency increased to 1.28 Hz and the average I_{sd} decreased by 6.8 nA (i.e., reflecting the increase of $C_{\text{K}^+}^{\text{ex}}$). Such spikes still showed up when measuring cardiomyocytes even with a bare SiNW-FET device without modifying Apt_{K^+} (Figure S7). In stark contrast, placing neurons on an $\text{Apt}_{\text{K}^+}/\text{SiNW-FET}$, or a bare SiNW-FET, did not show such a spike response (see the bottom trace in Figure S7). Therefore, these spikes are attributed to the beating characteristics of cardiomyocytes. To quantitate the elevation of $C_{\text{K}^+}^{\text{ex}}$ after an isoproterenol treatment, we calibrated the $\Delta V_{\text{g,K}^+}^{\text{cal}}$ of an $\text{Apt}_{\text{K}^+}/\text{SiNW-FET}$, prior to cell experiments, as a function of the extra C_{K^+} added into HBSS (Figure 4d). In Figure 4c, the ΔI_{sd} after isoproterenol stimulation was 6.8 nA, corresponding to $\Delta V_{\text{g,K}^+}^{\text{cal}}$ of 13.7 mV (*via* the $I_{\text{sd}}-V_{\text{g}}$ conversion shown in the inset of Figure 4d) and then to $\Delta C_{\text{K}^+}^{\text{ex}}$ of 7.4 mM (*via* the calibration curve in Figure 4d guided by the brown dashed lines). Such quick changes (within ~ 1 s in Figure 4c) in the average I_{sd} and heart beating frequency may be due to the concentration of isoproterenol applied (10 μM) was much higher than the EC_{50} (12.9 nM). Displayed in Figure S8 are a couple of additional tests with separate $\text{Apt}_{\text{K}^+}/\text{SiNW-FET}$ devices to measure the $\Delta C_{\text{K}^+}^{\text{ex}}$ released from other batches of the isoproterenol-stimulated cardiomyocytes, of which the results also give $\Delta C_{\text{K}^+}^{\text{ex}} \sim 6-8$ mM.

An elevation of $\Delta C_{\text{K}^+}^{\text{ex}}$ by several mM can enhance the neuronal excitability and even trigger the seizure-like responses in brain slices.³⁰ Some computational models also suggest that the $\Delta C_{\text{K}^+}^{\text{ex}}$ of a mM level can lead to changes in the firing pattern and network synchronization.^{8,9} In addition, the $\Delta C_{\text{K}^+}^{\text{ex}}$ in the mouse brain during the sleep-awake cycle is at a mM level detected by ion-selective microelectrodes.³ If the intracellular K^+ concentration maintains constant at 135 mM, according to the Nernst equation, the equilibrium potential of K^+ shifts from -81 to -47 and -59 mV when the $\Delta C_{\text{K}^+}^{\text{ex}}$ is 16

and 8 mM, respectively. Apparently, these elevations in $C_{\text{K}^+}^{\text{ex}}$ shift the resting membrane potential positively to enhance the neuronal electrical circuit and physiological brain activities. As our culture system is neuron-enriched, there might not have been plenty of astrocytes to buffer the excessive $\Delta C_{\text{K}^+}^{\text{ex}}$ when neurons were stimulated.³¹ This emphasizes the importance of astrocytes in maintaining the K^+ homeostasis in the brain.

CONCLUSIONS

The physiological electrolyte concentrations are an important health indicator. Both hypokalemia ($C_{\text{K}^+}^{\text{ex}} < 3.5$ mM) and hyperkalemia ($C_{\text{K}^+}^{\text{ex}} > 5.5$ mM) promote cardiac arrhythmia, resulting in heart failure.²⁹ Similarly, the accumulation of $C_{\text{K}^+}^{\text{ex}}$ in the heart will change the beat rate and even the pacemaker activity of the sinoatrial node.^{32,33} However, detecting the electrolyte concentrations in serum or tissues has been a time-consuming process and is not available for real-time emergent diagnosis.³⁴ An ion-selective microelectrode can adopt an ion-specific resin at the tip to monitor the concentration difference across this membrane; however, due to the diffusion limitation, this microelectrode has a slow response time and may receive interference from other ions.^{3,35}

In summary, our studies fully explored the advantages of a nanoelectronic aptasensor ($\text{Apt}_{\text{K}^+}/\text{SiNW-FET}$) in monitoring the physiological activities of excitable cells and confirmed the importance of K^+ efflux during electric activities in regulating the membrane potential. Therefore, this nanoelectronic device can be a vital tool to screen the factors that influence the activities of ion channels for pharmacological studies. In addition, a SiNW-FET device with different surface functionalizations, such as the $\text{Apt}_{\text{K}^+}/\text{SiNW-FET}$ of this work, can provide fast detections to reveal the amounts of the ion compositions in biological samples and even work as a tissue implant for a real-time health monitoring system. The real-time information about the ion fluctuation at specific regions of an organism can be an early warning before the onset of pathological responses like epilepsy and cardiac arrhythmia.

EXPERIMENTAL SECTION

Fabrication of MPC SiNW-FET Devices. The procedures used to produce MPC SiNW-FET devices can be found in our earlier publications.^{16,36} In short, monocrystalline boron-doped SiNWs of 20–30 nm in diameter were grown with assistance of catalytic gold nanoparticles in chemical vapor deposition reaction. A contact printing technique was used to deposit the as-synthesized p-type SiNWs onto a photoresist-patterned Si wafer of a 400 nm oxide layer. The MPC SiNW-FET devices were manufactured following standard photolithographic procedures. The electrodes were formed by thermal evaporation of metal layers ($\text{Ni}/\text{Al} = 70/100$ nm in thickness) on the regions predefined by a photomask of interdigitated patterns (Figure S1a). The MPC SiNW-FET devices were thermally annealed shortly after liftoff to achieve proper electrical contact between SiNWs and metal electrodes. The silica sheath ($\sim 2-3$ nm thick) on the SiNW surface could inhibit charge transfer or electrical leakage from a MPC SiNW-FET device to the analyte/buffer solution in biosensing measurements.

Immobilization of Apt_{K^+} on a MPC SiNW-FET Device. The detailed protocols for modifying the surface of SiNW-FET with DNA-aptamers can be found in our earlier publication.¹⁶ As shown in Figure 1b, the as-fabricated MPC SiNW-FET device was first modified using 3-aminopropyltrimethoxysilane (APTMS) and PTMS (molar ratio = 1:5). We then applied 3-maleimidobenzoyl *N*-hydroxysuccinimide (MBS) as a cross-linker to conjoin the amine group of APTMS to the Apt_{K^+} (3'-

GGTTGGTGTGGTTGGATTTT-SH-5') via 5'-SH of the Apt_K⁺. The surface modification of APTMS and PTMS with the molar ratio of 1:5 was used to control the number density of Apt_K⁺ on the SiNW-FET surface to render sufficient room for the proper folding of Apt_K⁺ during its binding with K⁺ ions in biosensing measurements. Typically, just ~17% of the SiNW surface has APTMS (amine groups) as the active sites for further modification with Apt_K⁺. Aside from adjusting the number density of Apt_K⁺, the modified PTMS molecules on the SiNW-FET additionally furnish a chemically inert surface to restrict non-specific binding in the biosensing experiments.

To demonstrate the successful immobilization of Apt_K⁺ on a SiO₂/Si surface, the fluorescein isothiocyanate dye (FITC) was tagged at the 3' end of Apt_K⁺ (referred to as FITC-Apt_K⁺) and the fluorescence image of the FITC-Apt_K⁺-immobilized SiO₂/Si surface was inspected. In Figure S2a, the uniform fluorescence image shows the homogeneous distribution of FITC-Apt_K⁺ on the SiO₂/Si surface, whereas no fluorescence was observed after modifying the SiO₂/Si surface with PTMS only (Figure S2b). Transfer curve ($I_{sd}-V_g$) measurements could also be used to investigate the surface modification of a SiNW-FET. In Figure S2c, the transfer curve of a SiNW-FET device shifted upward after Apt_K⁺ was modified onto the device, further supporting the surface functionalization of the SiNW-FET by Apt_K⁺. The upshift of the transfer curve after modifying the Apt_K⁺ was a typical electrostatic gating response of the p-type SiNW-FET against the negatively charged phosphate backbone of an oligonucleotide aptamer.

Electrical Measurements. The transfer curves of Apt_K⁺/SiNW-FETs were measured using a lock-in amplifier (Stanford Research System, SR830) with a modulation frequency of 79 Hz, a time constant of 100 ms, and a V_{sd} of 10 mV applied to the Apt_K⁺/SiNW-FET devices.¹⁶ In order to effectively detect K⁺ ions by Apt_K⁺/SiNW-FET, the K⁺-containing samples were dissolved in 10 mM of Tris buffer solution at pH 7.4 (prepared by mixing Tris HCl with Tris Base solution to achieve the desired pH value) for electrical measurements. The Debye-Hückel length of the as-prepared Tris buffer solution is ~3.1 nm without causing severe electrolytic screening in biosensing measurements. The sample solution was either loaded straightforwardly to a reservoir containing the Apt_K⁺/SiNW-FET chip surrounded by a PDMS wall (diameter: ~5 mm and height: ~10 mm) (Figure 1a), or driven by a syringe pump (KDS-101, KD Scientific) through a PDMS microfluidic channel (length: 6 mm, width: 500 μm, and height: 50 μm) coupled with the MPC/SiNW-FET chip. A Ag/AgCl electrode, submerged in the sample solution, was either utilized as a solution gate with the voltage supplied by a data acquisition system (National Instruments, DAQ-NI2110) or was held at ground potential in the biosensing experiments to reduce the electrical noise. After every K⁺-detection experiment, the K⁺ ions caught by Apt_K⁺/SiNW-FET were washed away by flushing Tris buffer to reset the Apt_K⁺/SiNW-FET device to its original surface condition without bound K⁺ ions.

Primary Culture of Cortical Neurons. The cortical neurons were isolated from Sprague Dawley rat embryos at E14.5 as described previously.³⁷ In brief, the procedure complied with the Animal Welfare Regulations and was approved by the Institutional Animal Care and Use Committee (Permit no. 103-30), National Taiwan University. The cells were plated at a density of 3×10^6 cells/mL and used for experiments at 7–10 days *in vitro*. Figure S1b shows an image of the cultured neurons.

Human Embryonic Stem Cell Culture and Differentiation. hESCs (H9 strain) were grown on a matrigel-coated culture dish in Essential E8 medium (Thermo Fisher Scientific) at 37 °C under a humidified atmosphere containing 5% CO₂. The medium was replaced daily, and a cardiac differentiation protocol was adopted as described previously.³⁸ Briefly, H9 was cultured in hESC medium to ~80% confluence. On the first day of the differentiation, H9 was treated with CHIR99021 (12 μM, a glycogen synthase kinase 3 inhibitor, Stem-RD Inc., USA) in RPMI1640 medium (Corning Inc. USA) supplemented with B27 minus insulin, GlutaMAX (2 mM), and Pen/Strep (100 U/mL) for 24 h. The CHIR99021 was not used after the second day. On the third day, IWR-1 (5 μM, WNT antagonist I,

Stemgent Inc., USA) was added into the medium and kept for 2 days (removed on the fifth day). On the eighth day, insulin was included in the cultured medium and then harvested on the 30th day for experiments.

Morphological Change and Intracellular Ca²⁺ Imaging of Differentiated Cardiomyocytes. Cultured cells grown on coverslips were incubated for 30 min in HBSS containing a Ca²⁺-sensitive fluorescent dye, Fluo2-AM (1 μM); after washing, the cells were placed on the recording chamber with the cells facing the bottom coverslip of the chamber at the stage of an inverted microscope (Olympus IX3 Microscope). To record the morphological changes, we captured the bright-field images at 10 Hz by a digital camera (Orca-Flash 4.0 digital CMOS camera, Hamamatsu). To record the fluorescence images, the excitation light was provided by a mercury lamp and the fluorescence images were captured by the same digital camera at 10 Hz. The whole system was controlled by the Olympus cellSens software. The frequency of the Ca²⁺ response was counted in a 1 min interval at the beginning of the recording and 1 min after the application of isoproterenol (10 μM).

Statistical Analysis. The mean and standard deviation (SD) were computed, and the Student's *t*-test was used to establish statistical significance. The sample size of each experiment is shown in the respective figures. Statistically significant differences are defined as $p < 0.05$.

■ ASSOCIATED CONTENT

Supporting Information

The Supporting Information is available free of charge at <https://pubs.acs.org/doi/10.1021/acsabm.1c00584>.

Materials and Reagents; dissociation constant; calculation of EC₅₀ by a Boltzmann sigmoidal function; electrical characterization of a representative MPC SiNW-FET device; immobilization of DNA-aptamers on the SiO₂/Si surface; calibration of an Apt_K⁺/SiNW-FET; differential responses of a PTMS/SiNW-FET and an Apt_K⁺/SiNW-FET to various C_K⁺; linear response of an Apt_K⁺/SiNW-FET to K⁺ ions in the presence of Na⁺ ions; non-specific binding of AMPA and DNQX on an Apt_K⁺/SiNW-FET device, comparison of the real-time responses of an Apt_K⁺/SiNW-FET to cardiac stem cells and cortical neurons; and fidelity of the electrical measurement by Apt_K⁺/SiNW-FETs in response to cardiomyocytes (PDF)

Cardiomyocyte-beating bright-field movie (AVI)

Cardiomyocyte calcium imaging before isoproterenol simulation (AVI)

Cardiomyocyte calcium imaging after isoproterenol simulation (AVI)

■ AUTHOR INFORMATION

Corresponding Authors

Chien-Yuan Pan – Department of Life Science, National Taiwan University, Taipei 10617, Taiwan; Email: cypan@ntu.edu.tw

Yit-Tsong Chen – Department of Chemistry, National Taiwan University, Taipei 10617, Taiwan; Institute of Atomic and Molecular Sciences, Academia Sinica, Taipei 10617, Taiwan; orcid.org/0000-0002-6204-8320; Email: ytchem@ntu.edu.tw

Authors

Ankur Anand – Department of Chemistry, National Taiwan University, Taipei 10617, Taiwan; Institute of Atomic and Molecular Sciences, Academia Sinica, Taipei 10617, Taiwan; orcid.org/0000-0003-2073-3845

Hui-Chiun Tseng – Department of Life Science, National Taiwan University, Taipei 10617, Taiwan

Hsu-Cheng Chiang – Department of Chemistry, National Taiwan University, Taipei 10617, Taiwan

Wan-Hsuan Hsu – Department of Life Science, National Taiwan University, Taipei 10617, Taiwan

Yi-Fan Liao – Department of Life Science, National Taiwan University, Taipei 10617, Taiwan; Institute of Physics, Academia Sinica, Taipei 11529, Taiwan

Serena Huei-An Lu – Department of Life Science, National Taiwan University, Taipei 10617, Taiwan

Su-Yi Tsai – Department of Life Science, National Taiwan University, Taipei 10617, Taiwan

Complete contact information is available at:

<https://pubs.acs.org/10.1021/acsabm.1c00584>

Author Contributions

The manuscript was written through contributions of all authors. All authors have given approval to the final version of the manuscript.

Notes

The authors declare no competing financial interest.

ACKNOWLEDGMENTS

This work was supported, in part, by the Ministry of Science and Technology (MOST) of Taiwan under Grant nos. 106-2113-M-002-022-MY3 and 107-2113-M-002-011-MY3 (Y.T.C.) and 106-2320-B-002-026 (C.Y.P.). Technical support from NanoCore, the Core Facilities for Nanoscience and Nanotechnology at Academia Sinica, is acknowledged. We would like to thank Mr. Hou-Jun Wang for his pilot study for characterizing the beat frequency of differentiated cardiomyocytes.

REFERENCES

- (1) Kadir, L. A.; Stacey, M.; Barrett-Jolley, R. Emerging Roles of the Membrane Potential: Action Beyond the Action Potential. *Front. Physiol.* **2018**, *9*, 1661.
- (2) Bean, B. P. The Action Potential in Mammalian Central Neurons. *Nat. Rev. Neurosci.* **2007**, *8*, 451–465.
- (3) Ding, F.; O'Donnell, J.; Xu, Q.; Kang, N.; Goldman, N.; Nedergaard, M. Changes in the Composition of Brain Interstitial Ions Control the Sleep-Wake Cycle. *Science* **2016**, *352*, 550–555.
- (4) Bellot-Saez, A.; Kékesi, O.; Morley, J. W.; Buskila, Y. Astrocytic Modulation of Neuronal Excitability through K⁺ Spatial Buffering. *Neurosci. Biobehav. Rev.* **2017**, *77*, 87–97.
- (5) Olabarria, M.; Noristani, H. N.; Verkhatsky, A.; Rodríguez, J. J. Concomitant Astroglial Atrophy and Astroglialosis in a Triple Transgenic Animal Model of Alzheimer's Disease. *Glia* **2010**, *58*, 831–838.
- (6) Li, J.; Gao, Z.; Kehoe, V.; Sinoway, L. I. Interstitial K⁺ Concentration in Active Muscle after Myocardial Infarction. *Am. J. Physiol.: Heart Circ. Physiol.* **2007**, *292*, H808–H813.
- (7) Martínez-Valverde, T.; Vidal-Jorge, M.; Montoya, N.; Sánchez-Guerrero, A.; Manrique, S.; Munar, F.; Pellegrini, M.-D.; Poca, M.-A.; Sahuquillo, J. Brain Microdialysis as a Tool to Explore the Ionic Profile of the Brain Extracellular Space in Neurocritical Patients: A Methodological Approach and Feasibility Study. *J. Neurotrauma* **2015**, *32*, 7–16.
- (8) Ullah, G.; Cressman, J. R., Jr.; Barreto, E.; Schiff, S. J. The Influence of Sodium and Potassium Dynamics on Excitability, Seizures, and the Stability of Persistent States: II. Network and Glial Dynamics. *J. Comput. Neurosci.* **2009**, *26*, 171–183.
- (9) Fröhlich, F.; Bazhenov, M.; Timofeev, I.; Steriade, M.; Sejnowski, T. J. Slow State Transitions of Sustained Neural Oscillations by Activity-Dependent Modulation of Intrinsic Excitability. *J. Neurosci.* **2006**, *26*, 6153–6162.
- (10) Patolsky, F.; Zheng, G.; Hayden, O.; Lakadamyali, M.; Zhuang, X.; Lieber, C. M. Electrical Detection of Single Viruses. *Proc. Natl. Acad. Sci. U.S.A.* **2004**, *101*, 14017–14022.
- (11) Pui, T.-S.; Agarwal, A.; Ye, F.; Tou, Z.-Q.; Huang, Y.; Chen, P. Ultra-Sensitive Detection of Adipocytokines with CMOS-Compatible Silicon Nanowire Arrays. *Nanoscale* **2009**, *1*, 159–163.
- (12) Chen, K.-I.; Li, B.-R.; Chen, Y.-T. Silicon Nanowire Field-Effect Transistor-Based Biosensors for Biomedical Diagnosis and Cellular Recording Investigation. *Nano Today* **2011**, *6*, 131–154.
- (13) Lin, T.-W.; Hsieh, P.-J.; Lin, C.-L.; Fang, Y.-Y.; Yang, J.-X.; Tsai, C.-C.; Chiang, P.-L.; Pan, C.-Y.; Chen, Y.-T. Label-Free Detection of Protein-Protein Interactions Using a Calmodulin-Modified Nanowire Transistor. *Proc. Natl. Acad. Sci. U.S.A.* **2010**, *107*, 1047–1052.
- (14) Wu, Y.-P.; Chu, C.-J.; Tsai, L.-C.; Su, Y.-W.; Chen, P.-H.; Moodley, M. K.; Huang, D.; Chen, Y.-T.; Yang, Y.-J.; Chen, C.-D. Detection of Electrically Neutral and Nonpolar Molecules in Ionic Solutions Using Silicon Nanowires. *Nanotechnology* **2017**, *28*, 165501.
- (15) Anand, A.; Liu, C.-R.; Chou, A.-C.; Hsu, W.-H.; Ulaganathan, R. K.; Lin, Y.-C.; Dai, C.-A.; Tseng, F.-G.; Pan, C.-Y.; Chen, Y.-T. Detection of K⁺ Efflux from Stimulated Cortical Neurons by an Aptamer-Modified Silicon Nanowire Field-Effect Transistor. *ACS Sens.* **2017**, *2*, 69–79.
- (16) Li, B.-R.; Hsieh, Y.-J.; Chen, Y.-X.; Chung, Y.-T.; Pan, C.-Y.; Chen, Y.-T. An Ultrasensitive Nanowire-Transistor Biosensor for Detecting Dopamine Release from Living PC12 Cells under Hypoxic Stimulation. *J. Am. Chem. Soc.* **2013**, *135*, 16034–16037.
- (17) Takenaka, S.; Juskowiak, B. Fluorescence Detection of Potassium Ion Using the G-Quadruplex Structure. *Anal. Sci.* **2011**, *27*, 1167–1172.
- (18) Rhodes, D.; Lipps, H. J. G-Quadruplexes and Their Regulatory Roles in Biology. *Nucleic Acids Res.* **2015**, *43*, 8627–8637.
- (19) Ishikawa, F. N.; Curreli, M.; Chang, H.-K.; Chen, P.-C.; Zhang, R.; Cote, R. J.; Thompson, M. E.; Zhou, C. A Calibration Method for Nanowire Biosensors to Suppress Device-to-Device Variation. *ACS Nano* **2009**, *3*, 3969–3976.
- (20) Ida, R.; Wu, G. Direct NMR Detection of Alkali Metal Ions Bound to G-Quadruplex DNA. *J. Am. Chem. Soc.* **2008**, *130*, 3590–3602.
- (21) Alberts, B.; Johnson, A.; Lewis, J.; Raff, M.; Roberts, K.; Walter, P. *Molecular Biology of the Cell*; Garland Science: New York, 2008, pp 667–670.
- (22) Dai, W.-M.; Egebjerg, J.; Lambert, J. D. C. Characteristics of AMPA Receptor-Mediated Responses of Cultured Cortical and Spinal Cord Neurons and Their Correlation to the Expression of Glutamate Receptor Subunits. *Br. J. Pharmacol.* **2001**, *132*, 1859–1875.
- (23) Jane, D. E.; Hoo, K.; Kamboj, R.; Deverill, M.; Bleakman, D.; Mandelzys, A. Synthesis of Willardiine and 6-Azawillardiine Analogs: Pharmacological Characterization on Cloned Homomeric Human AMPA and Kainate Receptor Subtypes. *J. Med. Chem.* **1997**, *40*, 3645–3650.
- (24) Fearnley, C. J.; Roderick, H. L.; Bootman, M. D. Calcium Signaling in Cardiac Myocytes. *Cold Spring Harbor Perspect. Biol.* **2011**, *3*, a004242.
- (25) Eng, G.; Lee, B. W.; Protas, L.; Gagliardi, M.; Brown, K.; Kass, R. S.; Keller, G.; Robinson, R. B.; Vunjak-Novakovic, G. Autonomous Beating Rate Adaptation in Human Stem Cell-Derived Cardiomyocytes. *Nat. Commun.* **2016**, *7*, 10312.
- (26) Stiles, G. L.; Lefkowitz, R. J. Cardiac Adrenergic Receptors. *Annu. Rev. Med.* **1984**, *35*, 149–164.
- (27) Brito-Martins, M.; Harding, S. E.; Ali, N. N. β_1 - and β_2 -Adrenoceptor Responses in Cardiomyocytes Derived from Human Embryonic Stem Cells: Comparison with Failing and Non-Failing Adult Human Heart. *Br. J. Pharmacol.* **2008**, *153*, 751–759.
- (28) Kline, R. P.; Morad, M. Potassium Efflux in Heart Muscle during Activity: Extracellular Accumulation and Its Implications. *J. Physiol.* **1978**, *280*, 537–558.

- (29) Weiss, J. N.; Qu, Z.; Shivkumar, K. Electrophysiology of Hypokalemia and Hyperkalemia. *Circ.: Arrhythmia Electrophysiol.* **2017**, *10*, No. e004667.
- (30) Somjen, G. G. *Ions in the Brain: Normal Function, Seizures, and Stroke*; Oxford University Press: New York, 2004; pp 202–209.
- (31) Noori, H. R. The Impact of the Glial Spatial Buffering on the K^+ Nernst Potential. *Cogn. Neurodyn.* **2011**, *5*, 285–291.
- (32) Zhang, H.; Yang, Z.; Yang, L.; Kong, S. Effects of High Extracellular K^+ in Atrium on Pacemaker Activity of Sinoatrial Node. *Pak. J. Pharm. Sci.* **2014**, *27*, 2041–2046.
- (33) Weiss, J.; Shine, K. I. Effects of Heart Rate on Extracellular $[K^+]$ Accumulation during Myocardial Ischemia. *Am. J. Physiol.: Heart Circ. Physiol.* **1986**, *250*, H982–H991.
- (34) Chapp, A. D.; Schum, S.; Behnke, J. E.; Hahka, T.; Huber, M. J.; Jiang, E.; Larson, R. A.; Shan, Z.; Chen, Q.-H. Measurement of Cations, Anions, and Acetate in Serum, Urine, Cerebrospinal Fluid, and Tissue by Ion Chromatography. *Physiol. Rep.* **2018**, *6*, No. e13666.
- (35) Nicholson, C. Ion-Selective Microelectrodes and Diffusion Measurements as Tools to Explore the Brain Cell Microenvironment. *J. Neurosci. Methods* **1993**, *48*, 199–213.
- (36) Patolsky, F.; Zheng, G.; Lieber, C. M. Fabrication of Silicon Nanowire Devices for Ultrasensitive, Label-Free, Real-Time Detection of Biological and Chemical Species. *Nat. Protoc.* **2006**, *1*, 1711–1724.
- (37) Wu, M.-P.; Kao, L.-S.; Liao, H.-T.; Pan, C.-Y. Reverse Mode Na^+/Ca^{2+} Exchangers Trigger the Release of Ca^{2+} from Intracellular Ca^{2+} Stores in Cultured Rat Embryonic Cortical Neurons. *Brain Res.* **2008**, *1201*, 41–51.
- (38) Chang, C.-W.; Chang, C.-C.; Hsia, K.-C.; Tsai, S.-Y. Generation of FHL2 Homozygous Knockout Lines from Human Embryonic Stem Cells by CRISPR/Cas9-Mediated Ablation. *Stem Cell Res.* **2018**, *27*, 21–24.

Supporting Information

Significant Elevation in Potassium Concentration Surrounding Stimulated Excitable Cells Revealed by an Aptamer-Modified Nanowire Transistor

Ankur Anand,^{a,d} Hui-Chiun Tseng,^b Hsu-Cheng Chiang,^a Wan-Hsuan Hsu,^b Yi-Fan Liao,^{b,c} Serena Huei-An Lu,^b Su-Yi Tsai,^b Chien-Yuan Pan,^{b,*} Yit-Tsong Chen^{a,d,*}

^aDepartment of Chemistry, National Taiwan University, Taipei 10617, Taiwan

^bDepartment of Life Science, National Taiwan University, Taipei 10617, Taiwan

^cInstitute of Physics, Academia Sinica, Taipei 11529, Taiwan

^dInstitute of Atomic and Molecular Sciences, Academia Sinica, Taipei 10617, Taiwan

* Corresponding author. Email: cypan@ntu.edu.tw, or ytchem@ntu.edu.tw

S1. Materials and Reagents

Trizma hydrochloride (Tris-HCl), 3-aminopropyltrimethoxysilane (APTMS), propyltrimethoxysilane (PTMS), dimethyl sulfoxide (DMSO), and 3-maleimidobenzoic acid *N*-hydroxysuccinimide (MBS) were purchased from Sigma Aldrich. Other chemicals were also procured commercially: single-strand DNA-aptamer from MDBio, polydimethylsiloxane (PDMS) from Sil-More Industrial Ltd., and Hank's balanced salt solution (HBSS) from Gibco. Dulbecco's modified Eagle's medium and all other reagents for cell culture were supplied from Invitrogen. Deionized water (>18 M Ω ·cm) obtained from a purification system (Millipore Synergy) was used throughout the experiments.

S2. Dissociation Constant

The dissociation constant (K_d) of the K^+ -Apt $_{K^+}$ complex was determined by a least-squares fit of the $C_{K^+} / \Delta V_{g, K^+}^{cal}$ vs. C_{K^+} data (in the inset of Figure 2b) to the Langmüir adsorption isotherm model:

$$\frac{C_{K^+}}{\Delta V_{g, K^+}^{cal}} = \frac{1}{\Delta V_{g, K^+}^{cal, max}} \cdot C_{K^+} + \frac{1}{\Delta V_{g, K^+}^{cal, max}} \cdot K_d \quad (\text{Eq. S1})$$

where the relative $\Delta V_{g, K^+}^{cal}$ is defined as $\Delta V_{g, K^+}^{cal} (\%) = (\Delta V_{g, K^+}^{cal} - \Delta V_{g, 0}^{cal}) / \Delta V_{g, 0}^{cal} \times 100 (\%)$,

$\Delta V_{g, 0}^{cal}$ is the calibrated response at $C_{K^+} = 0$ M that induces no detectable signal, and $\Delta V_{g, K^+}^{cal, max}$

is the saturated calibrated response at high C_{K^+} .

S3. Estimation of EC₅₀ Using a Boltzmann Sigmoidal Function

The EC₅₀ value was determined by fitting the dose response curve (Figure 3d) to a Boltzmann sigmoidal function with Origin 9.1 (OriginLab).

$$y = \frac{A_1 - A_2}{1 + e^{-\frac{(x-x_0)}{dx}}} + A_2 \quad (\text{Eq. S2})$$

where, A_1 , and A_2 are the values of the lower and upper limits on the dose-response curve, respectively, x is C_{AMPA} , x_0 is the dose corresponding to the midpoint (i.e., EC_{50}) between A_1 and A_2 , and dx denotes the slope of the dose-response curve.

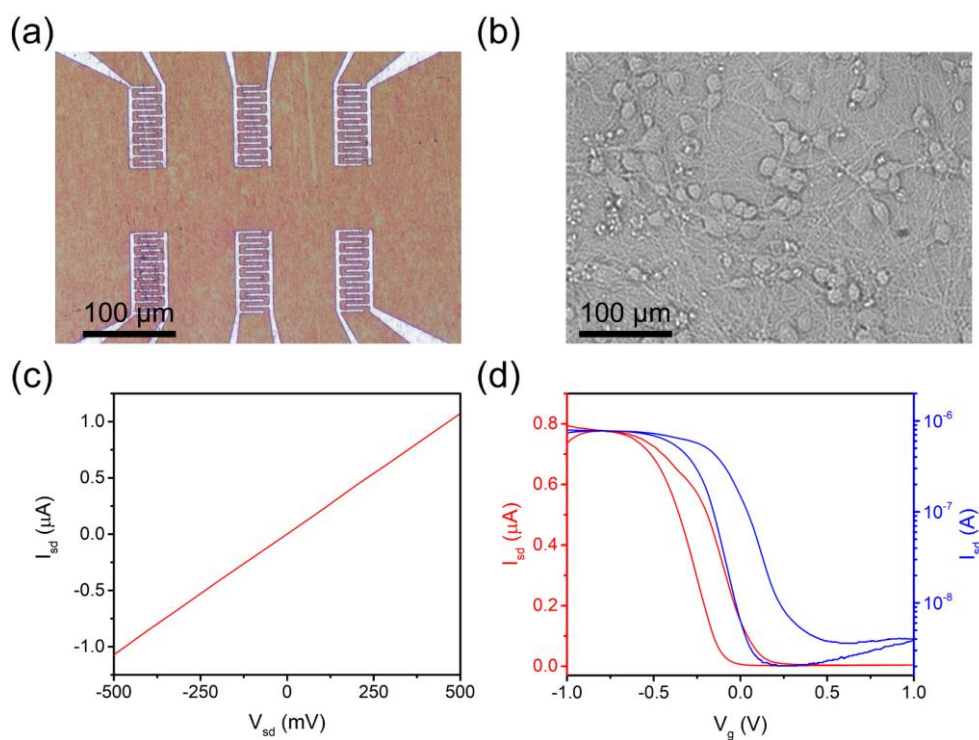


Fig. S1. Electrical characterization of a representative MPC SiNW-FET device. (a) A single chip contains six sets of MPC SiNW-FETs. Every MPC SiNW-FET set comprises tens to hundreds of p-type single-crystalline boron-doped SiNWs (20–30 nm in diameter for each SiNW) as conducting channels, which were located underneath and placed between the interdigitated source and drain electrodes. (b) An image of primary cultured rat embryonic cortical neurons. (c) The representative output curve (I_{sd} – V_{sd}) of a bare MPC SiNW-FET was measured to show an ohmic contact between SiNWs and electrodes. The output curve was scanned in an ambient condition with a digital multimeter (Keithley 6487). (d) The transfer curve (I_{sd} – V_g) of a bare MPC SiNW-FET was measured in $1\times$ PBS buffer solution (containing 10 mM Na_2HPO_4 , 1.8 mM KH_2PO_4 , 137 mM NaCl, and 2.7 mM KCl, pH 7.4) using a lock-in amplifier (Stanford Research System, SR830) at V_{sd} of 10 mV, a modulation frequency of 79 Hz, and a time constant of 100 ms. The solution gate voltage (V_g), scanned from -1 V to +1 V and back to -1 V, was applied to a Ag/AgCl reference electrode *via* a data acquisition system (National Instruments, DAQ-NI2110). The obtained transfer curve is plotted on a linear (red) or a logarithmic (blue) scale.

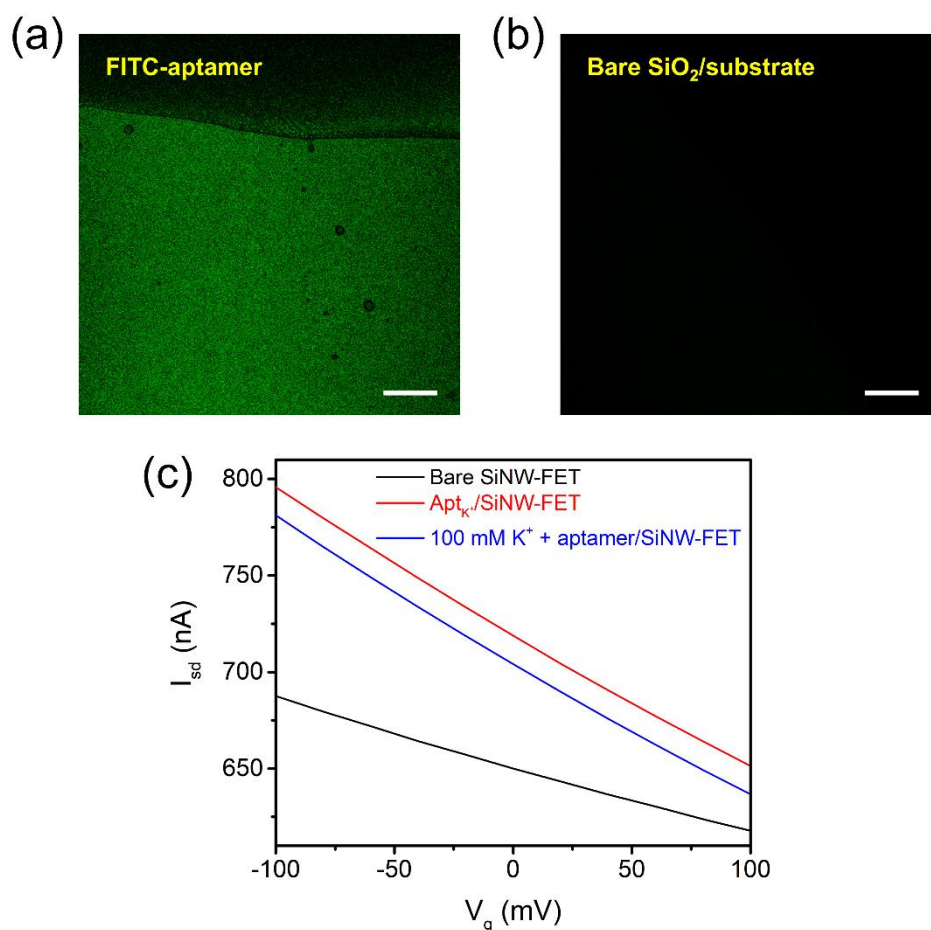


Figure S2. Demonstration of the successful immobilization of Apt_{K⁺} on SiO₂/Si surface. (a) Fluorescent image of an FITC-tagged-Apt_{K⁺}-modified SiO₂/Si substrate. The modification procedures are described in Figure 1c and Experimental Section of the main text. Scale bar: 100 μ m. (b) A SiO₂/Si substrate modified with only PTMS shows no fluorescence. Scale bar: 100 μ m. (c) The transfer curves of a MPC SiNW-FET device in a Tris buffer were recorded with different surface conditions: (i) a bare SiNW-FET (black trace), (ii) an Apt_{K⁺}/SiNW-FET (red trace), and (iii) an Apt_{K⁺}/SiNW-FET bound with K⁺ ions (blue trace). The upward/downward shifts of the transfer curve are caused by an electrostatic gating effect on the p-type SiNW-FET device. While the up-shift of the transfer curve (relative to the black curve of a bare SiNW-FET) after modifying Apt_{K⁺} (the red curve) was due to the negatively charged backbone of Apt_{K⁺}, the down-shift of the transfer curve after binding K⁺ ions to the Apt_{K⁺}/SiNW-FET (the blue curve) was caused by the positive K⁺ ions.

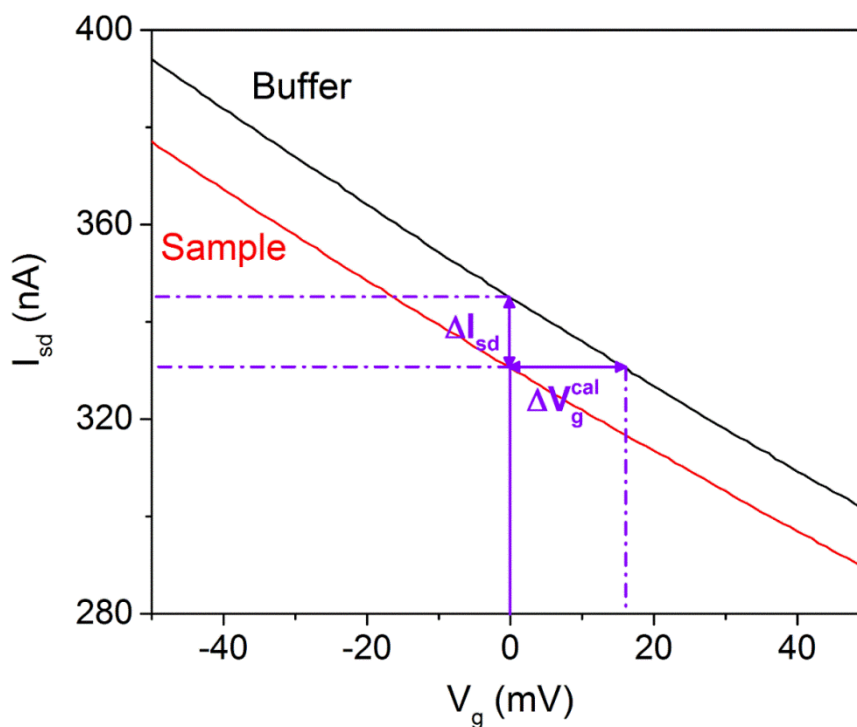


Figure S3. To avoid device-to-device variation in the detection sensitivity with different Apt_{K⁺}/SiNW-FET devices, the measured current change due to the binding of K⁺ to an Apt_{K⁺}/SiNW-FET (ΔI_{sd} at $V_g = 0$ mV, relative to the buffer solution) was converted to the changes in V_g (termed the calibrated response and represented by ΔV_g^{cal}) according to the transfer curve of the MPC SiNW-FET device used.

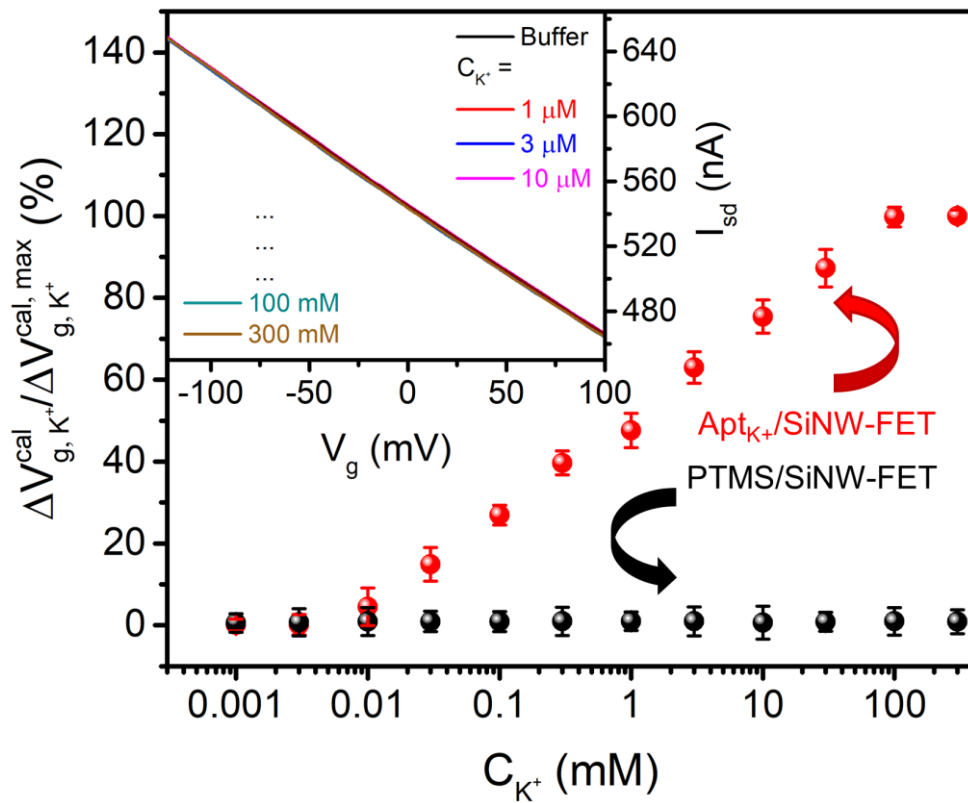


Figure S4. A semi-logarithmic plot of the normalized calibrated responses of an Apt_{K⁺}/SiNW-FET (red dots, with the data points taken from Figure 2a of the main text) and a PTMS/SiNW-FET (black dots) in response to various C_{K⁺}. The inset shows the measured transfer curves of a PTMS/SiNW-FET as a function of C_{K⁺}, indicating no significant response of the PTMS/SiNW-FET to K⁺ ions.

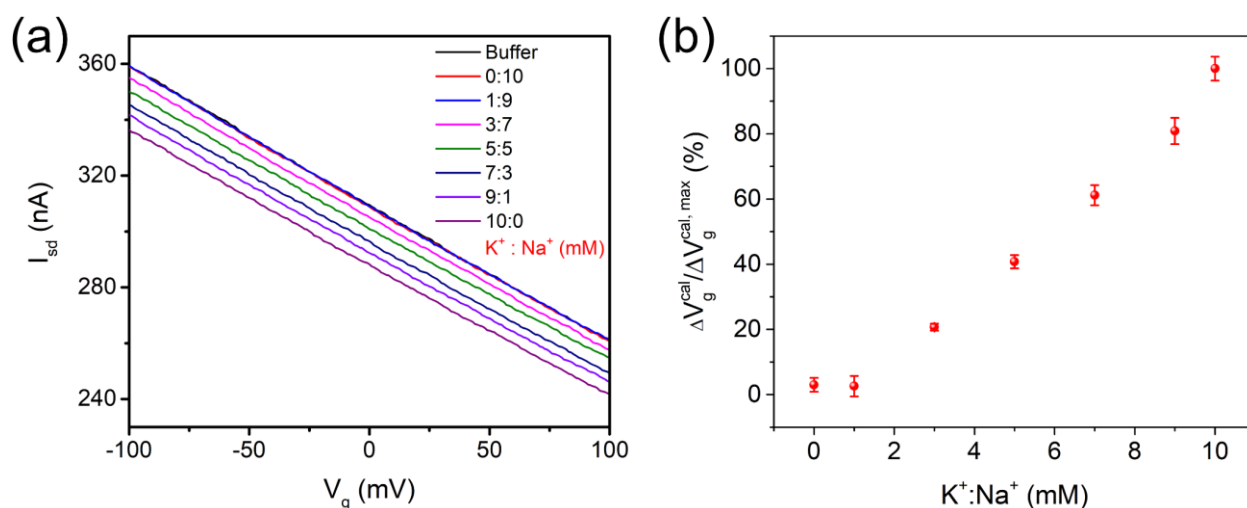


Figure S5. An $Apt_{K^+}/SiNW$ -FET was used to probe K^+ ions in the presence of Na^+ ions. (a) The transfer curves of an $Apt_{K^+}/SiNW$ -FET were measured in a mixture of Na^+ and K^+ ions (at different $K^+ : Na^+$ concentration ratios, but with a constant total concentration of 10 mM) dissolved in Tris buffer at pH 7.4. (b) The measured $\Delta V_g^{cal} / \Delta V_g^{cal, max}$ as a function of different $K^+ : Na^+$ concentration ratios. The ΔV_g^{cal} data were taken from Panel (a) at $V_g = 0$ mV. The data presented are the mean \pm standard deviation from three independent experiments.

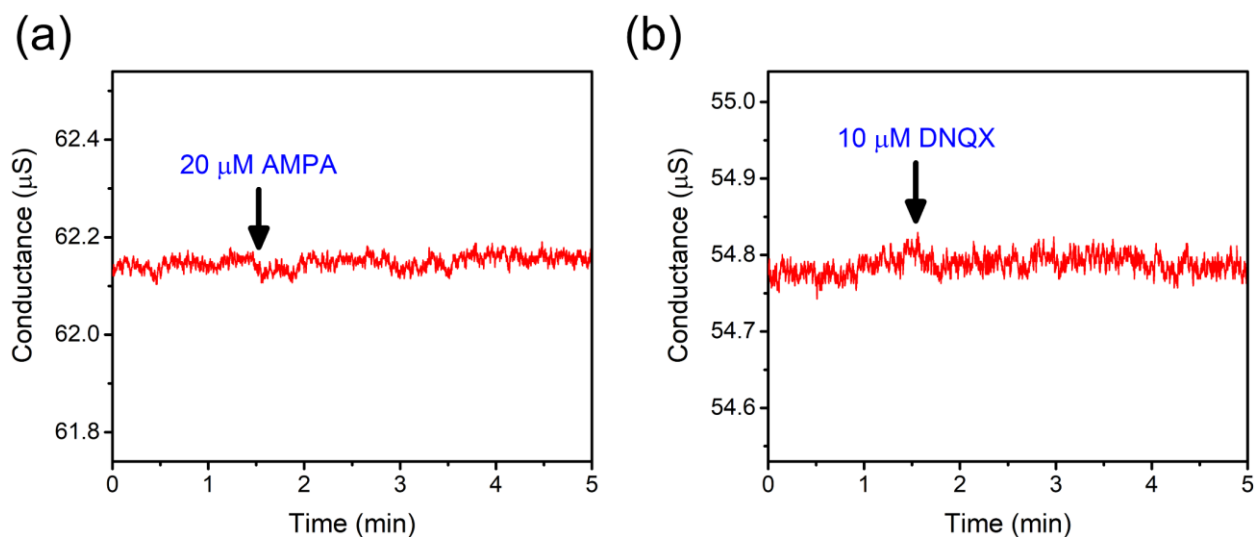


Figure S6. In the absence of cortical neurons, no conductance changes were observed in an Apt_{K+}/SiNW-FET by adding (a) AMPA (20 μM) and (b) DNQX (10 μM) on the Apt_{K+}/SiNW-FET device. The arrows indicate the sample applications.

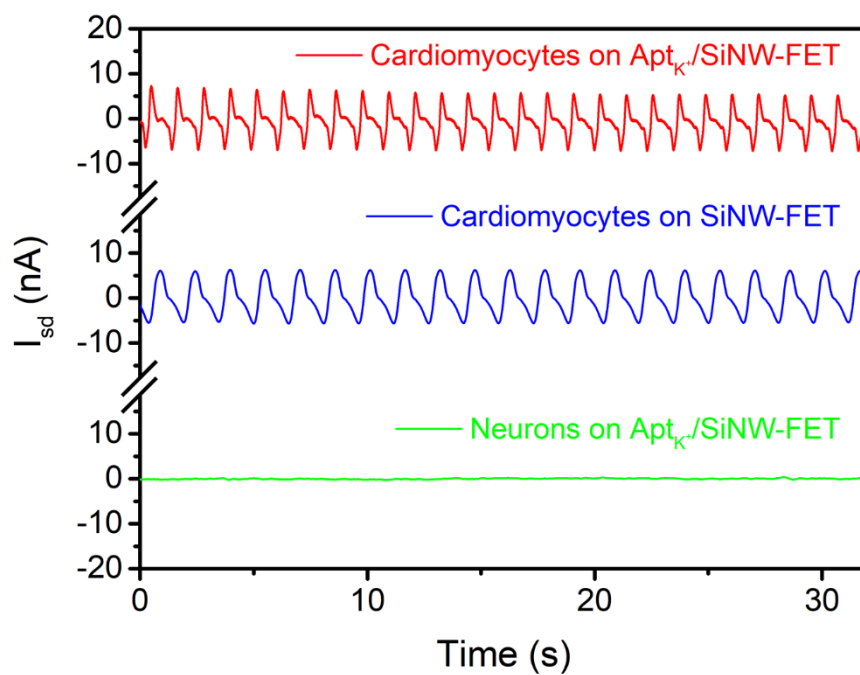
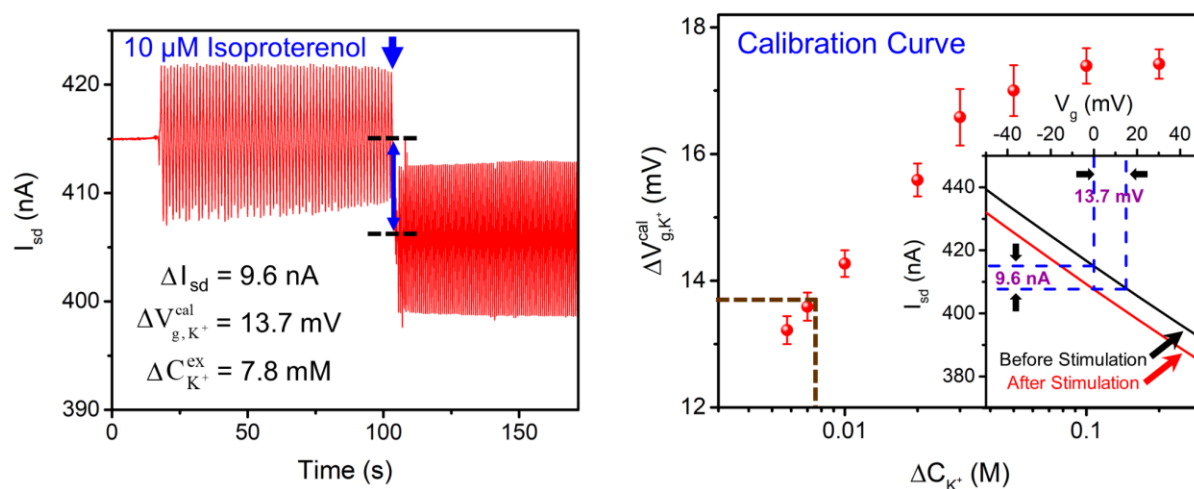


Figure S7. Transient spikes appeared on the I_{sd} recording by placing cardiomyocytes on an Apt_K⁺/SiNW-FET (red trace) or a bare SiNW-FET (blue trace). In sharp contrast, no spikes showed up by placing neurons on the same Apt_K⁺/SiNW-FET (green trace).

Device 2



Device 3

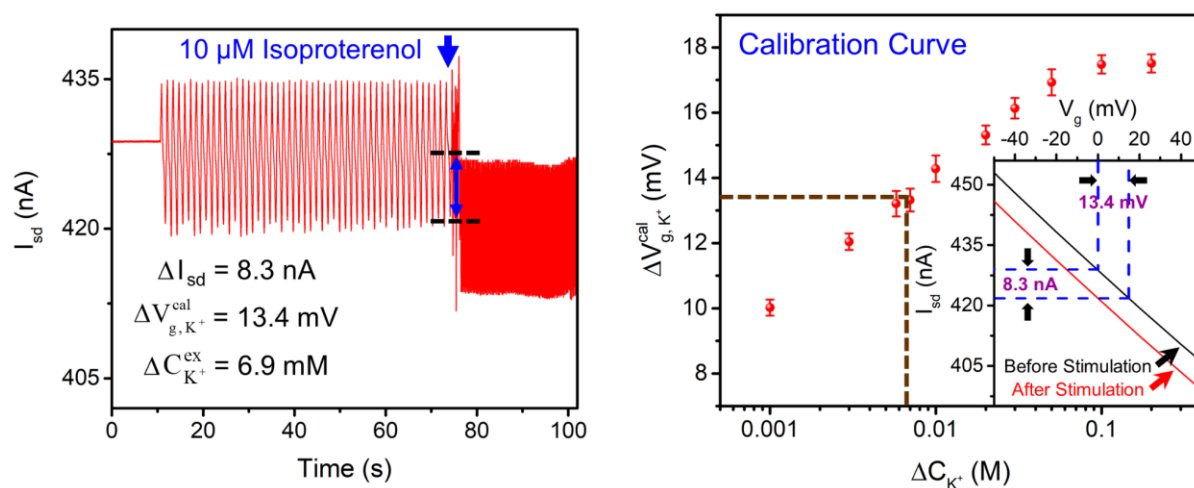


Figure S8. The similar changes in beating frequency and $\Delta C_{K^+}^{\text{ex}}$ of isoproterenol-stimulated cardiomyocytes were detected by two more $\text{Apt}_{K^+}/\text{SiNW-FET}$ devices (i.e., by Device 2 and Device 3, other than by Device 1 presented in Figure 4(c)–(d) of the main text). These observations show the fidelity of the electrical measurements for isoproterenol-stimulated cardiomyocytes by $\text{Apt}_{K^+}/\text{SiNW-FET}$. The procedures for data analysis are the same as those described in Figure 4(c)–(d) of the main text.

Supplementary Videos

Supplementary Video 1: Cardiomyocyte beating bright-field movie (.avi).

Supplementary Video 2: Cardiomyocyte calcium imaging before Isoproterenol simulation (.avi).

Supplementary Video 3: Cardiomyocyte calcium imaging after Isoproterenol simulation (.avi).